arXiv:1605.09478v2 [cond-mat.soft] 2 Aug 2016

Jamming on curved surfaces

Christopher J. Burke and Timothy J. Atherton
Department of Physics and Astronomy, Tufts University, 574 Boston Avenue, Medford, Massachusetts 02155, USA

Colloidal and other granular media experience a transition to rigidity known as jamming if the fill fraction is increased beyond a critical value. The resulting jammed structures are locally disordered, bear applied loads inhomogenously, possess the minimal number of contacts required for stability and elastic properties that scale differently with volume fraction to crystalline media. Here the jamming transition is studied on a curved ellipsoidal surface by computer simulation, where shape evolution leads to a reduction in area, crowding the particles and preventing further evolution of the surface. The arrested structures can be unjammed and the surface further evolved iteratively, eventually leading to a rigid metric-jammed state that is stable with respect to motion of the particles and some specified space of deformations of the manifold. The structures obtained are compared with those obtained in flat space; it is found that jammed states in curved geometries require fewer contacts per particle due to the nonlinearity of the surface constraints. In addition, structures composed of soft particles are compressed above the jamming point. It is observed that relatively well-ordered but geometrically frustrated monodispersed packings share many signatures of disordered bidispersed packings.

I. INTRODUCTION

Jamming is a transition to rigidity that occurs at high density, low temperature and low applied stress in granular media, glasses and foams[1]. Jammed structures are mechanically stable and behave as a solid in the bulk, but lack crystalline order. Particularly well-defined is the jamming point J that occurs at a critical packing density ϕ_c at zero temperature and stress; at this point, packings are stable with respect to an infinitesimal applied stress.

Packings at the jamming point possess a number of remarkable features: first, are typically disordered according to some measure of local crystalline order[2]. In two dimensions, this is quantified by the hexatic order parameter,

$$\psi_6 = \langle \exp(i6\theta) \rangle \,, \tag{1}$$

where the average is taken over the nearest neighbors. Second, they are *isostatic*, or possess the minimal number of contacts required for mechanical stability[3]. This number in Euclidean space is calculated by matching the number of degrees of freedom, ND for a packing of N spheres in D dimensions, to the number of constraints $ZN/2$ if each particle has, on average, Z contacts with neighboring particles. This yields $Z = 2n$, i.e. $Z = 4$ for 2D. In contrast, a crystalline hexagonal packing has $Z = 6$. Third, if the particles themselves are deformable, the structure can be compressed beyond the jamming point. These disordered jammed packings exhibit a number of scaling laws[4–7]. In particular, the scaling of elastic moduli with density is found to be very different from that of crystalline solids, due to the abundance of soft modes.

Powerful theoretical tools have been developed to classify the nature of the jammed structures. For hard particles, Torquato and Stillinger*[8]* proposed a taxonomy of jamming based on the space of feasible motions available to the constituent particles: A packing is *locally jammed*, the least stringent category, if no particles are able to move while the others remain fixed; it is *collectively jammed* if no subset of particles is movable with the remainder held in place; it is *strictly jammed* if no collective subset of the particles can be moved at the same time as a volume conserving deformation of the container. The category to which a configuration belongs can be determined numerically by solving a linear program, for which efficient algorithms exist permitting the classification of structures with large numbers of particles[9].

In contrast to hard particle packings, packings of particles with soft, finite range potentials can be compressed beyond the jamming point. For disordered packings (typically bidispersed packings in 2D or 3D, or monodipsersed packings which are able to avoid crystallization in 3D), as the density is increased above the jamming point, a number of specific mechanical properties are observed which distinguish them from crystalline packings. They show an excess of low-frequency vibrational modes (in contrast to the Debye law behavior of ordered solids[10]), as seen in a number of glassy and disordered systems[5, 11–13]. They also exhibit critical scaling laws as the density is increased above the jamming point[5]. This is true for the contact number Z, as well as the bulk modulus B and the shear modulus G. These scaling properties reveal the nonlinear nature of packings near the jamming point. In flat space, monodispersed packings in 2D are highly crystalline — disordered monodispersed packings can be produced only under extreme circumstances[14]. However, for packings in a curved 2D space, crystalline order is frustrated by the surface geometry, necessitating defects and inducing strain in the crystalline regions of the packing[15–19]. The question arises, then, of how geometric frustration affects the mechanical properties at the jamming point.

In this work, we consider the situation where jamming occurs on a curved surface. One situation where this might happen is if colloidal particles are trapped by sur-

face tension on the surface of an emulsion droplet and either the size of the droplet is reduced or the shape deformed to one with lower surface area. At sufficient density, the particles become crowded and arrest further evolution of the surface. This mechanism can stabilize a variety of arrested shapes, including bispheres[20] and ellipsoids[19]. The questions we address in this paper are: 1) are these states jammed? and 2) how does curvature affect the mechanical properties near the jamming point? Packings of particles on a curved surface are also important in other applications, for example in spherical codes, i.e. packings of particles on the surface of a sphere of arbitrary dimensions, which are useful as error correcting codes[21].

The paper is organized as follows: first studying hard particles, in section II A we adapt the linear program of ref. [9] to curved spaces; in section II B we apply it to arrested packings, allowing us to evolve them toward an ultimately arrested state and compare their features with jammed configurations in Euclidean space; we examine in section II C whether the packings are isostatic and find that the criteria for this must be modified in the presence of curvature. Packings of soft particles on curved surfaces are studied in section II D; we compare the properties of disordered bidispersed packings to relatively well ordered but geometrically frustrated monodispersed packings. Brief conclusions are presented in section III.

II. RESULTS

A. Unjamming arrested packings

We simulate N hard particles of radius r that move diffusively on a prolate ellipsoidal surface of fixed volume and aspect ratio a that evolves from $a_0 > 1$ toward the spherical state $a = 1$ as the simulation progresses. The centroids of the particles are fixed rigidly to the surface and, as the surface evolves, particles are kept on it using constraint forces imposed through a Lagrange multiplier. Overlaps caused by surface evolution are resolved by gradient descent. If the initial coverage of particles is sufficiently high, the particles become crowded and, at some aspect ratio a_f, arrest further evolution of the surface. The algorithm features adaptive time-stepping to resolve the dynamics near the point of arrest and further details are given in the Methods section. We refer to the output of this algorithm as an *arrested* structure; the central question of this section is to determine whether they are also jammed. The arrested structures studied here all have an aspect ratio near $a = 4$.

To test for jamming, we adapt the linear program developed by Donev *et. al.*[9], which aims to find a prototypical unjamming motion $\Delta\mathbf{x}$ by applying a random force $\mathbf{F}$ to the packing. The force $\mathbf{F}_i$ experienced by particle i is drawn from a spherically symmetric gaussian distribution of unit variance. The program maximizes the virtual work,

$$\max_{\Delta\mathbf{x}} \mathbf{F}^{\mathrm{T}} \cdot \Delta\mathbf{x}, \tag{2}$$

subject to an interpenetrability constraint for each pair of particles (i, j),

$$(\Delta\mathbf{x}_i - \Delta\mathbf{x}_j)^{\mathrm{T}} \cdot \hat{\mathbf{x}}_{ij} \geq 2r \tag{3}$$

where $\hat{\mathbf{x}}_{ij}$ is a unit vector pointing from the center of particle i to particle j, and also subject to an overall bound on the motion,

$$\|\Delta\mathbf{x}\| < X_{max}. \tag{4}$$

The appropriate surface constraint is obtained from the level set representation of the surface $f(\mathbf{x}) = 0$ by MacLaurin expansion,

$$f(\mathbf{x} + \Delta\mathbf{x}) = f(\mathbf{x}) + \frac{\partial f}{\partial \mathbf{x}} \cdot \Delta\mathbf{x} + ... = 0,$$

and noting that $\frac{\partial f}{\partial \mathbf{x}}$ is parallel to the local surface normal $\mathbf{N}$. Hence, the linearized surface constraints are,

$$\mathbf{N}_i \cdot \Delta\mathbf{x}_i = 0 \tag{5}$$

where $\mathbf{N}_i$ is the surface normal at the ith particle center and corresponding to allowing motion of the particle in the local tangent plane. Finally, because ellipsoids possess a trivial rotational symmetry, we also constrain the angular momentum of the motion $\Delta\mathbf{x}$ about the symmetry axis $\hat{\mathbf{z}}$ to suppress the corresponding motion,

$$\sum_i \hat{\mathbf{z}} \cdot (\mathbf{x}_i \times \Delta\mathbf{x}_i) = 0. \tag{6}$$

We note that the use of a linear constraint for the surface is hence a more egregious approximation than, say, the interpenetrability condition because, unless the surface happens to be locally flat, any finite $\Delta\mathbf{x}$ takes the particle away from the surface and hence violates the true nonlinear constraint. To compensate for this, we restrict the bound on the motion $X_{max} \leq r$, and, having found an unjamming motion, test that it is feasible within the nonlinear constraint.

A typical arrested configuration is depicted in fig. 1. In fig. 1A, the particles are colored by the hexatic order parameter ψ_6, revealing large regions of approximately crystalline order separated by disordered regions. Applying the linear program described above to this configuration reveals the prototypical unjamming motion depicted in fig. 1B. Executing this motion along the surface opens gaps in the packing. By alternating application of the linear program to unjam the system with further relaxation of the surface, it is possible to evolve the system further towards the equilibrium state. Fig. 1C shows a typical example of the change in area as a function of iteration number, showing that after a few applications of the linear program, the system arrives at an *ultimately arrested* state beyond which further evolution is precluded.

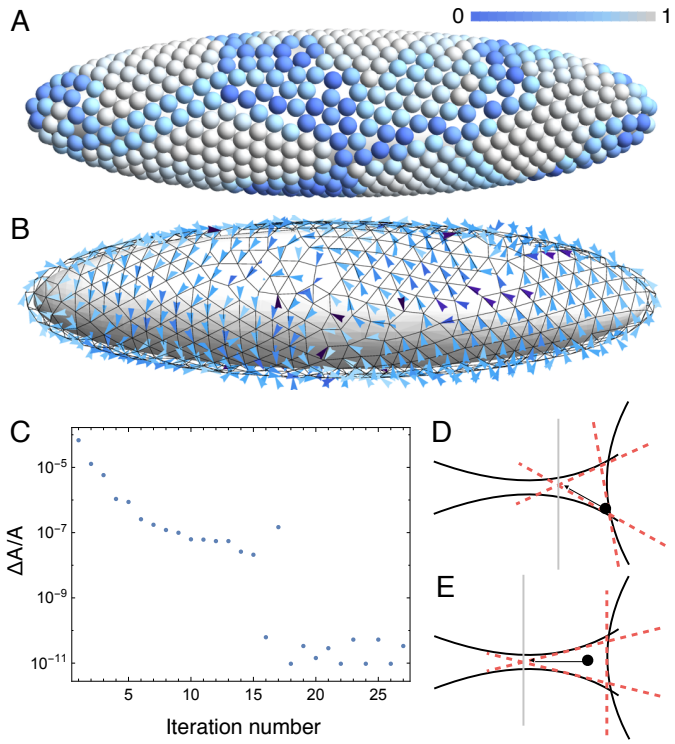

Figure 1. **A** An arrested structure produced by evolution of an ellipsoidal surface at constant volume with the particles colored by the hexatic order parameter ψ_6. **B** Unjamming motion found for this structure using the linear program. Executing the unjamming motion permits further evolution of the surface. **C** Plot of relative area decrease in successive unjamming and evolution steps. **D** Arrested packings often have particles at the edge of the feasible region of moves, the jamming polytope, for a particle (solid black line) for which the linear approximant (red dashed lines) is relatively poor. **E** Preconditioning the configuration through gradient descent moves particles to the center of the jamming polytope, for which the linear approximant has greater fidelity.

We found that the process of successive unjamming and relaxing could be accelerated by a preconditioning step in which an artificial energy functional is minimized with respect to the particle positions by gradient descent. The functional used supplements the hard particle constraint with a short range repulsive pairwise auxiliary potential,

$$V = \begin{cases} \infty & x \leq 2r \\ (x - x_c)^2 \left(\log(x - 2r) - \log(x_c)\right) & 2r < x < x_c \\ 0 & x_c \leq x \end{cases} \tag{7}$$

where x is the center-to-center particle distance and $x_c = 2.1r$ is a distance cutoff beyond which particles do not interact. Note that the logarithmic form of this auxiliary potential diverges as particles come in contact with one another, preserving the hard-particle constraint. Preconditioning the particle positions by gradient descent of the auxiliary potential enables the linear program

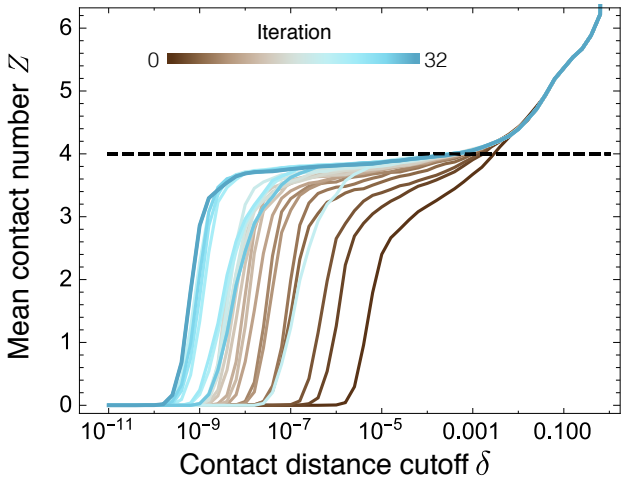

Figure 2. Mean number of contacts Z as a function of the contact cutoff distance δ. Note that the leftward shift is not monotonic: this is due to the alternating use of the linear program and the full energy minimization; the energy minimization results in more even spacing and thus larger interparticle distance on average.

to more effectively find unjamming motions.

The reason for the improvement due to the preconditioning steps may be understood by considering the set of feasible motions available to the particles, referred to in the literature as the *jamming polytope*[22]. As shown in fig. 1D, the output of the arrest algorithm tends to produce packings with particles that are locally close to the edge of the jamming polytope, where the linearized version of the jamming polytope is a poor approximation and artificially constricted. Preconditioning by gradient descent tends to move particles into the center of the jamming polytope where the linear approximation is better and hence allows the linear program to more effectively find an unjamming motion, as in fig. 1E.

In addition to the linear program, a full energy minimization of the auxiliary potential can be performed and often leads to an unjamming motion. However, this is computationally expensive and thus full energy minimization steps are only attempted when the linear program fails to uncover an unjamming motion.

B. Are arrested packings jammed?

We now wish to determine whether the arrested or ultimately arrested states resemble a jammed state. A powerful tool to do so is to examine the contact network. Two particles are defined to be in contact at a cutoff distance δ if the distance between them $x < 2r + \delta$. A plot of the average number of contacts Z as a function of the cutoff distance possesses a characteristic shape for a jammed state[23]: $Z = 0$ for low δ; at some characteristic *contact lengthscale* δ_0, Z quickly rises to the isostatic value; once $\delta \geq r$ Z diverges like δ^D where D is the

dimensionality of the space.

We show in fig. 2 the contact number distribution $Z(\delta)$ for a sequence of successive preconditioning, unjamming and surface evolution steps described above. After the initial unjamming step, the contact lengthscale is $\delta_0 \sim 10^{-5}$. Following unjamming and evolution, δ_0 decreases and approach a limiting curve with $\delta_0 \sim 10^{-9}$.

For this ultimately arrested configuration, the linear program is no longer able to find a finite unjamming motion. The state is therefore at least *collectively jammed* according to the taxonomy of [8], but this classification is too permissive because it does not account for deformations of the manifold on which the packing is embedded. The more restrictive epithet of strictly jammed is not directly applicable here, because the jamming occurs on a compact surface without boundaries to deform. Rather, the packing is also jammed with respect to volume conserving and area-reducing deformations of the ellipsoid; the jamming is caused by change in the underlying metric of the space as surface relaxation occurs.

We therefore propose to call the ultimately arrested configurations *metric jammed* states, which we define to mean that the packing is jammed with respect to simultaneous collective motions of the particles and some well-defined set of deformations of the manifold. This restriction parallels that of strict jamming, which does not permit arbitrary deformations of the boundary, but rather requires the allowed deformation to conserve volume. Hence, the initially arrested states are not jammed, but rather evolve toward the metric jammed state upon repeated application of the linear program to unjam them and relaxation of the surface.

C. Criteria for isotaticity

We now compare features of the metric jammed state to those of jammed states in Euclidean space. Most notably, the contact number distributions $Z(\delta)$, even in the limit of metric jamming, lack the clear plateau observed in [23]. This is because jammed packings contain some fraction of underconstrained particles that are free to move within a cage created by their neighbors. These are referred to as *rattlers* and should be excluded from the average used to create the plot of $Z(\delta)$[9].

Rattlers are identified based on the number of contacts they make with their neighbors — a particle needs three contacts which are not in the same hemisphere to be constrained. To count contacts for the purpose of identifying rattlers, we again choose a cutoff separation distance below which particles are in contact, but we consider the separation between a particle an its neighbors from every point available to a particle while its neighbors are held fixed. We do this because two particles may be close in the simulation output, but one of the particles may be able to move a significant distance. For example, a rattler may be close to a neighbor and may be identified as being in contact with that neighbor, while that contact does not contribute to the mechanical stability of the packing. We give details of the contact identification process in the supplementary material.

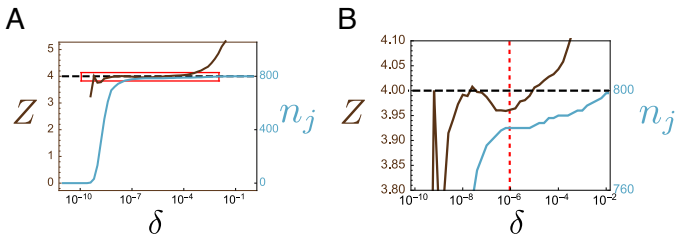

Figure 3. A) Plot of Z versus δ with rattlers removed (brown), alongside the number of non-rattlers n_j, i.e. the number of particles in the packing which are locally jammed. B) Zooming in on the highlighted region in (A), we see that at the value of δ where the number of non-rattlers begins to plataeu, the packing appears to be hypostatic as indicated by a value of $Z < 4$.

Having identified rattlers, we replot $Z(\delta)$ with rattlers excluded, as well as the number of particles which are not identified as rattlers (fig. 3). For Z, the intermediate region is greatly flattened, more closely resembling the plateau observed in Euclidean space[23]. Fascinatingly, at $\delta = 10^{-6}$, where the number of non-rattlers begins to plateau, the metric jammed packing has $Z = 3.962$ and has not reached the expected isostatic value of $Z = 4$. As δ is increased, we do not see $Z = 4$ until $\delta = 10^{-5}$, a full order of magnitude higher.

This is a striking result for two reasons: First, for a system with such a high degree of hexatic order, we might expect an average contact number near $Z = 6$. We don't see this because curvature of the surface induces strain in the crystalline regions of the packing[15] and the hard particle constraints prevent local compression; rather the lattice is slightly oblique and hence each particle has only four contacts in the crystalline regions of the packing.

Second, packings with $Z < 4$ should be hypostatic according to the constraint counting argument above. To further explore this, we generated an ensemble of metric jammed packings at particle number N, with 30 results at each value. We display the number of missing contacts in fig. 4, using $\delta = 10^{-6}$ as our contact cutoff. A few packings are found that have an excess of contacts, but most display an apparent deficit. Notice that there is an apparent bound on the number of missing contacts that grows linearly with N, with an approximate slope of 0.014. We also display data for bidispersed packings. The particle diameter ratio is 1.4, a value which results in a high degree of disorder[5]. Interestingly, both monodispersed and bidispersed packings appear to share a similar lower bound on the contact number, despite the monodispersed packings having a high degree of hexagonal ordering compared to the bidisperse packings.

The reason for the missing contacts is the nonlinear surface constraint. To show this, we present a toy example shown in fig. 5A. Five spherical particles are arranged

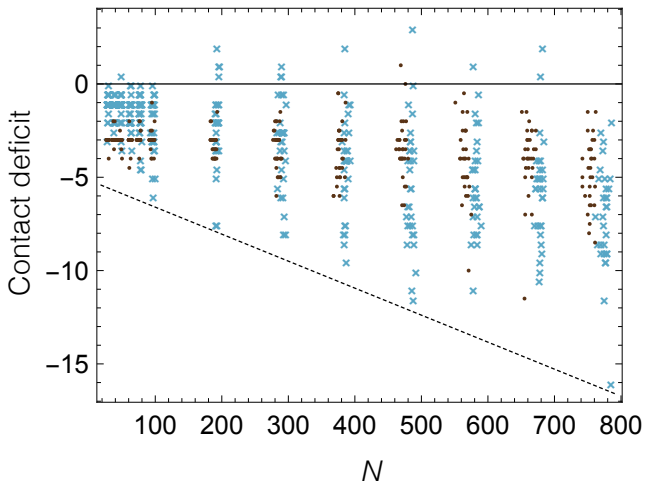

Figure 4. Contact deficit, the number of contacts minus the number expected in Euclidean space, for an ensemble of configurations with different N (not counting rattlers). Blue Xs represent monodispersed packings and brown points represent bidispersed packings. The dashed line shows the apparent lower bound.

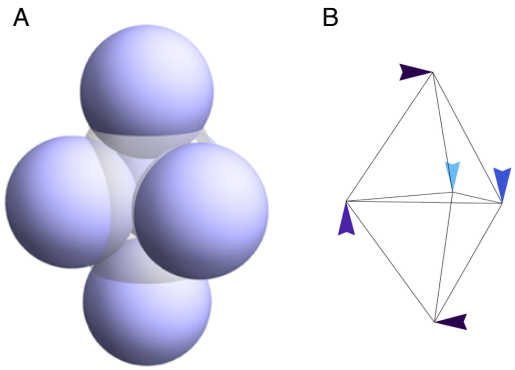

Figure 5. **A** Arrested packing of 5 particles with the center of masses positioned on the surface of an ellipsoid of aspect ratio $\sqrt{2}$ at the vertices of a triangular bipyramid. **B** The linear programming finds this unjamming motion, representing rotation about the ellipsoid, but this motion is not feasible within the nonlinear surface constraint.

at the vertices of a triangular bipyramid with equilateral faces; these are embedded on a commensurate ellipsoid of aspect ratio $\sqrt{2}$. The total number of contacts is 9; the two particles on the top and bottom touch three other particles and the three particles around the edge touch four others. The constraint counting argument in Euclidean space would predict 10 contacts were needed for isostaticity.

Applying the linear program to the example in fig. 5A reveals an apparent unjamming motion shown in fig. 5B that attempts to rotate the configuration about an axis parallel to the equatorial plane of the ellipsoid. This motion is, however, totally prevented by the nonlinear surface constraint. The structure is therefore metric jammed according to the above definition, but it is clear that the constraint counting for isostaticity must be modified to account for the curved surface. This is reminiscent of the situation where non-spherical particles are jammed in Euclidean space[24].

D. Soft particles

To generate packings of soft particles, we again employ the dynamic packing algorithm, replacing the hard particle interactions with a compact Hertzian interaction,

$$V_{ij} = \frac{\epsilon}{2/5}\left(1 - \frac{r_{ij}}{\sigma_{ij}}\right)^{2/5} \Theta\left(\frac{\sigma_{ij}}{r_{ij}} - 1\right)$$

where ϵ determines the energy scale, r_{ij} is the distance between the centroids of particles i and j, σ_{ij} is the sum of the radii of the particles, and Θ is the Heaviside step function enforcing a finite interaction range. Both monodispersed packings and bidipsersed packings with a radius ratio of 1.4 are produced. The surface relaxation proceeds past the point where all particles are overlapping, creating over-jammed configurations — the packings become rigid near an aspect ratio of $a = 4.0$, and the surface evolution continues to an aspect ratio of $a = 3.0$. All packings consist of $N = 800$ particles. We apply an energy minimization to the final packing, fixing the surface geometry and using a conjugate gradient method[25]. From these energy minimized configurations, we expand the packing quasistatically (i.e. minimizing the energy after each small expansion step) at fixed aspect ratio. This allows us to find the jamming point packing fraction ϕ_c corresponding to the initial energy minimized configuration (as ϕ_c is a property specific to a given packing, not a universal value[5]), while also generating packing fractions in the intermediate range of packing fractions to study the mechanical behavior of the packings as a function of $\phi - \phi_c$.

First we investigate the vibrational modes of the packings. To calculate vibrational modes along the surface, we impose a harmonic energy penalty for particle motions normal to the surface, with an energy scale much larger than the particle interaction energy scale. We then calculate the Hessian matrix of the packing energy with respect to the particle coordinates in 3D and diagonalize it to find eigenfrequencies and eigenmodes, and ignore modes normal to the surface which are easily identifiable due to their much higher frequencies.

Figure 6 shows the density of vibrational frequencies $D(\omega)$ for both monodispersed and bidispersed packings at various values of $\phi - \phi_c$. We see that as ϕ approaches ϕ_c, the so-called boson peak[26], an excess of low frequency modes, shifts towards $\omega = 0$, and at very low packings fractions ($\phi - \phi_c = 10^{-5}$), there is a finite density of states extending down to $\omega = 0$. This is a signature of marginal stability: below ϕ_c, the particles are not

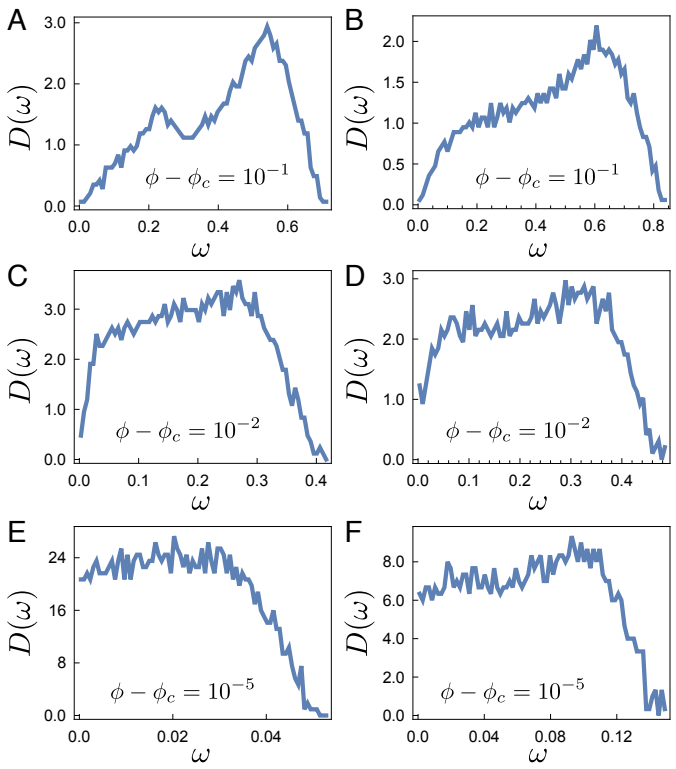

Figure 6. Density of states of vibrational modes for a (A,C,E) monodipsersed and (B,D,F) bidispersed packing. In both cases, as the packing fraction nears ϕ_c, an excess of modes is observed for at low ω. Notably, the monodispersed packing does not show Debye law behavior, despite the high degree of hexagonal order. Frequencies are in units of $\sqrt{\epsilon}/r$, where r is the larger radius for bidisperse packings.

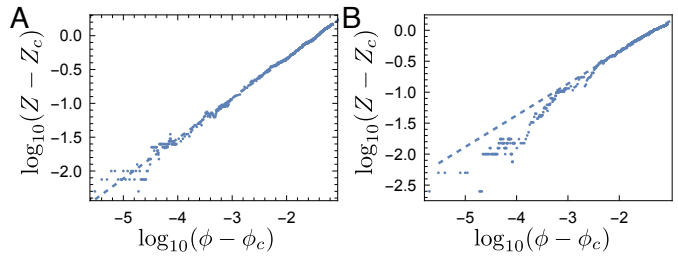

Figure 7. Scaling of the average contact number versus packing fraction above the jamming point for (A) a monodispersed packing and (B) a bidispersed packing. For the monodipsersed case, the data follows a power law, as shown by the dashed line. For the bidipsersed case, the data deviates from a power law at lower packing fraction, but the power law fit for data with $\phi - \phi_c > 10^{-3}$ describes the data well.

in contact and all vibrational modes are zero-frequency modes. As a packing approaches the jamming point from above, it develops an abundance of very low frequency modes.

Next we look at the scaling of $Z - Z_c$ with respect to $\phi - \phi_c$, where Z_c is the contact number at which packings are marginally stable. For the monodispersed case, we see a power law behavior with exponent 0.60 ± 0.06, larger than the value of 0.5 usually seen in disordered packings[5]. For the bidispersed case, we find that a power law behavior holds at higher packings fractions: taking the power law fit for data with $\phi - \phi_c > 10^{-3}$, we find a power law exponent of 0.50 ± 0.02, consistent with previous results for disordered packings. However, the data tends to deviate form this power law behavior closer to the jamming point. Data for a single monodispersed and a single bidispersed packing is shown in fig. 7. Uncertainties are the standard deviations in the fit exponents among 30 packings.

Finally, we investigate the scaling of the elastic moduli of packings near jamming. Disordered jammed systems exhibit a number of nonlinear elastic behaviors. These can be seen by comparing the instantaneous response and infinite-time response of their bulk and shear moduli. The instantaneous moduli are calculated by applying a uniform compression or shear and then calculating the response of the system pressure. The infinite-time moduli are calculated by applying the same deformation, but then minimizing the configuration energy before calculating the system response. If the system behaves linearly, then the deformation will scale or shear the configuration's local energy landscape but will not change its structure and the configuration will still be at a local energy minimum. In disordered jammed materials, however, a difference is observed between the instantaneous and infinite-time response: for the bulk modulus, both the instantaneous response B_0 and the infinite-time response B_∞ show a power law which scales as $(\phi - \phi_c)^{\alpha-2}$, where α is the exponent of the interaction potential (e.g. 5/2 for Hertzian interactions.) Despite having the same power law exponent, the power laws have different coefficients such that $B_\infty < B_0$. The difference is more extreme for the shear moduli G_0 and G_∞, which have different power law exponents: $G_0 \propto (\phi - \phi_c)^{\alpha-2}$ and $G_\infty \propto (\phi - \phi_c)^{\alpha-1.5}$[5].

The bulk and shear moduli can be derived from the pressure tensor. The pressure tensor of the packing can be calculated by[27]

$$p_{\alpha\beta} = A^{-1} \sum r_{ij\alpha} \frac{r_{ij\beta}}{r_{ij}} \frac{dV}{dr_{ij}}$$

where A is the surface area, V is the full configuration energy, and $r_{ij\alpha}$ is the component of $\vec{r}_{ij}$ along the surface coordinate alpha (we take $\vec{r}_{ij}$ in 3D and take the projection along the surface tangent vectors $\vec{t}_\theta$ and $\vec{t}_\phi$ in the polar and azimuthal directions, respectively, at both positions $\vec{r}_i$ and $\vec{r}_j$ and use the average between the two points.) From this, the bulk modulus can be calculated from the pressure, $B = \phi \frac{dp}{d\phi}$, where $p = \frac{1}{2} \sum_\alpha p_{\alpha\alpha}$. The shear modulus is given by $G = \frac{d\Sigma}{d\gamma}$ where $\Sigma = p_{\theta\phi}$ and γ is the applied shear. The shear is applied by twisting the configuration around the ellipsoid symmetry axis such that $\frac{ds_\phi}{ds_\theta}$ is constant (where s_θ and s_ϕ are arc lengths

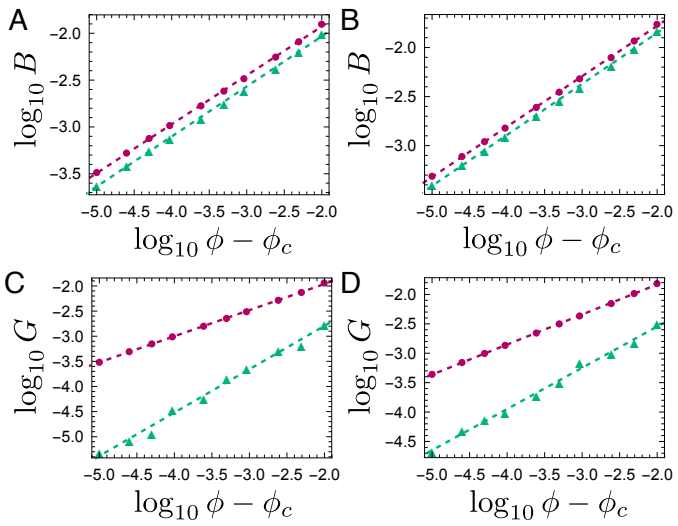

Figure 8. (A, B) Log-log plots of the bulk modulus for a (A) monodispersed and (B) bidispersed packing. (C, D) Log-log plots of the shear modulus for a (A) monodispersed and (B) bidispersed packing. Data for the instantaneous responses B_0 and G_0 are shown as red circles, and the infinite-time responses B_∞ and G_∞ are shown as green triangles. Dashed lines are power law fits. In both A and B, the B_∞ is lower than B_0, with the same scaling exponent. In C and D, the scaling exponent changes between G_0 and G_∞. These are all indications of nonlinear elastic behavior.

along the polar and azimuthal directions), i.e. there is a uniform shear rate across the surface. After applying a shear we fix the positions of several particles near the poles of the surface to ensure that the packing will not relax back completely after the energy minimization, and we exclude the fixed particles (and the area they cover) from the pressure tensor calculation. Results for the elastic moduli are given in units of ϵ/r^2 (where r is the larger particle radius in bidispersed packings.)

Table I reports the power law fitting parameters for the bulk and shear modulus. For the bulk modulus, we see the same behavior in the relatively well ordered monodispersed packings as we see in bidipsersed packings: fitting a power law of the form $B = B^0(\phi - \phi_c)^\beta$ to the data we see an exponent of about 0.5 (as expected for a Hertzian potential) for both B_0 and B_∞, and we see that $B_\infty < B_0$ to a significant degree. For the shear modulus fits of the form $G = G^0(\phi - \phi_c)^\gamma$, we do see a change in the exponent γ for both monodipsersed and bidispersed packings. Curiously, this exponent is about $\gamma = 0.72$ for both cases, signifying a smaller change between the instantaneous and infinite time shear modulus than seen previously in the literature[5]. Data and power law fits are shown for a pair of example configurations in fig. 8.

It is rather surprising that monodipsersed packings on a 2D surface share so many properties with disordered packings, given that the monodispersed packings are relatively well ordered. There are two effects, both stemming from geometric frustration, which may lead to the packings exhibiting these properties near the jamming point. First, the surface curvature as well as its topology necessitate topological defects in the packing[16]. These defects correspond to localized regions of disorder. Second, the curvature causes strain in the nearly-hexagonal packing[15]. Thus, instead of the surface being covered by a perfect hexagonal lattice with each particle in contact with six neighbors, the lattice is slightly oblique and most particles have four contacts — allowing for the average contact number $Z \approx 4$ as seen in sec. II C.

III. CONCLUSION

In section II A we adapt the algorithm of [9] to search for unjamming motions in packings of hard particles on curved surfaces. Applying this algorithm to arrested packings generated by relaxing an ellipsoidal surface at fixed volume, we find in section II B that these arrested packings are generally not jammed. By repeated unjamming the packings and further relaxing the surface, we artificially age the packings towards a metric jammed state, that is, the final packings are stable to both collective particle motions and further surface evolution.

Upon careful investigation (II C) we see that the metric jammed packings typically have an average contact number $Z < 4$, where $Z = 4$ is the isostatic contact number required for stability of sphere packings in flat 2D space. This deficit in the contact number is explained by the surface curvature imposing nonlinear constraints on the packing, in addition to the constraints due to interparticle contacts. For packings of increasing particle number, an increasing number of apparently "missing" contacts is observed. This trend is currently unexplained. Ideally one could derive an analytical prediction for the number of missing constraints based on the number of particles, likely from geometric and topological considerations (perhaps analogous to the result that crystalline packings on curved surfaces have a net topological defect charge based on their topology[28]).

In section II D, we turn to packings of soft particles compressed past the jamming point. By comparing monodispersed and bidispersed packings, we see that despite the high degree of hexagonal ordering in monodispersed packings, their mechanical properties near the jamming point resemble those of highly disordered bidispersed packings, due to geometric frustration induced by the curved surface.

Another goal for future work would be to further improve the unjamming linear program for curved surfaces. Possible improvements include using quadratic constraints, or using a quadratic program instead of a linear program. This would allow the program to better handle the nonlinear surface constraints, and thus avoid finding false unjamming motions. Another important improvement would be to incorporate surface deformations. Currently, surface evolution and particle unjamming steps are handled separately. Ideally, they would

		B^0	β	G^0	γ
Monodispersed	Instantaneous	0.134 ± 0.004	0.522 ± 0.004	0.123 ± 0.005	0.519 ± 0.004
	Infinite-time	0.111 ± 0.007	0.532 ± 0.007	0.05 ± 0.03	0.72 ± 0.07
Bidispersed	Instantaneous	0.179 ± 0.003	0.514 ± 0.002	0.167 ± 0.006	0.513 ± 0.003
	Infinite-time	0.155 ± 0.004	0.518 ± 0.003	0.08 ± 0.03	0.72 ± 0.06

Table I. Scaling law fits for the bulk and shear moduli of both monodispersed and bidispersed packings of 800 particles on ellipsoids of aspect ratio 3.0. Scaling fits are of the form $B = B^0(\phi - \phi_c)^\beta$ and $G = G^0(\phi - \phi_c)^\gamma$. For both monodispersed and bidispersed packings, we see a drop in B^0 from the instantaneous to the infinite-time response, while β does not change significantly. Again for both monodispersed and bidispersed packings, we see a change in γ from near 0.5 to 0.72. Both of these behaviors indicate that monodispersed packings show the same nonlinear behavior as bidispersed packings. Uncertainties are the standard deviations in the fit parameters among 30 packings.

be combined into one unjamming program.

METHODS

Dynamic packing algorithm

Arrested packings are produced by an algorithm that simulates diffusive motion of particles on an evolving surface. N particles of fixed radius r are initially placed with their centers of mass on an ellipsoidal surface of aspect ratio a by random sequential absorption. The simulation then proceeds by a sequence of *diffusion steps* and *surface evolution steps*: diffusion steps evolve the particle positions according to a Langevin equation,

$$\vec{x}_i'(t + \Delta t_p) = \vec{x}_i(t) + \vec{\eta}_i\sqrt{2D\Delta t_p},$$

where η_i is a random noise term sampled from a gaussian distribution of unit variance along the tangent plane of the surface at $\vec{x}_i$. Particle centroids are constrained to remain on the surface by Lagrange multipliers. Surface evolution steps relax the ellipsoidal surface towards a spherical ground state such that the area decreases exponentially as a function of simulation time,

$$A(t) = A_s + (A_e - A_s)\exp(-\lambda t),$$

where A_s is the area of the final spherical state, A_e is the area of the initial ellipsoid and λ is the relaxation constant. Particles are reprojected onto the surface along the normal direction, and where reprojection causes overlap of particles, a relaxation step is performed to remove the overlap. To do so, an artificial potential is applied to the particles,

$$V_{\text{overlap}} = \begin{cases} r^2 - rx & x < r \\ 0 & x \geq r \end{cases}$$

and the resulting energy functional is minimized by conjugate gradient. The simulation employs dynamic time-stepping to ensure accuracy as the arrest point is approached.

ACKNOWLEDGMENTS

The authors wish to thank Aleksandar Donev and Andrea Liu for helpful discussions. We would also like to thank the Research Corporation for Science Advancement for financial support through a Cottrell Award.

[1] Andrea J. Liu and Sidney R. Nagel. The Jamming Transition and the Marginally Jammed Solid. *Annual Review of Condensed Matter Physics*, 1(1):347–369, aug 2010.

[2] Anuraag R. Kansal, Salvatore Torquato, and Frank H. Stillinger. Diversity of order and densities in jammed hard-particle packings. *Physical Review E - Statistical, Nonlinear, and Soft Matter Physics*, 66(4):1–8, 2002.

[3] Cristian F. Moukarzel. Isostatic Phase Transition and Instability in Stiff Granular Materials. *Physical Review Letters*, 81(8):1634–1637, aug 1998.

[4] Corey O'Hern, Stephen Langer, Andrea Liu, and Sidney Nagel. Random Packings of Frictionless Particles. *Physical Review Letters*, 88(7):075507, jan 2002.

[5] Corey S. O'Hern, Leonardo E. Silbert, Andrea J. Liu, and Sidney R. Nagel. Jamming at zero temperature and zero applied stress: The epitome of disorder. *Physical Review E*, 68(1):011306, jul 2003.

[6] J. a. Drocco, M. B. Hastings, C. J. Olson Reichhardt, and C. Reichhardt. Multiscaling at Point J: Jamming is a Critical Phenomenon. *Physical Review Letters*, 95(8):088001, aug 2005.

[7] C. J. Olson Reichardt and C. Reichardt. Fluctuations, jamming, and yielding for a driven probe particle in disordered disk assemblies. *Phys. Rev. E*, 82(5):051306, 2010.

[8] S. Torquato and F. H. Stillinger. Multiplicity of Generation, Selection, and Classification Procedures for Jammed Hard-Particle Packings. *Journal of Physical Chemistry*, 105:11849–11853, 2001.

[9] Aleksandar Donev, Salvatore Torquato, Frank H. Stillinger, and Robert Connelly. A linear programming algorithm to test for jamming in hard-sphere packings. *Journal of Computational Physics*, 197(1):139–166, 2004.

[10] Charles Kittel. *Introduction to Solid State Physics*. Wiley, New York, 1995.

[11] Leonardo E Silbert, Andrea J Liu, and Sidney R Nagel. Vibrations and Diverging Length Scales Near the Unjamming Transition. *Physical Review Letters*, 098301(August):098301, 2005.

[12] Leonardo E. Silbert, Andrea J. Liu, and Sidney R. Nagel. Normal modes in model jammed systems in three dimensions. *Physical Review E - Statistical, Nonlinear, and Soft Matter Physics*, 79(2):1–7, 2009.

[13] Daniel M Sussman, Carl P Goodrich, Andrea J Liu, and Sidney R Nagel. Disordered surface vibrations in jammed sphere packings. *Soft Matter*, 11(14):2745–2751, 2015.

[14] Steven Atkinson, Frank H Stillinger, and Salvatore Torquato. Existence of isostatic , maximally random jammed monodisperse hard-disk packings. *Proceedings of the National Academy of Sciences*, 111(52):18436–18441, 2014.

[15] H. S. Seung and David R. Nelson. Defects in flexible membranes with crystalline order. *Physical Review A*, 38(2):1005–1018, jul 1988.

[16] Mark Bowick, David Nelson, and Alex Travesset. Interacting topological defects on frozen topographies. *Physical Review B*, 62(13):8738–8751, oct 2000.

[17] William T M Irvine, Vincenzo Vitelli, and Paul M Chaikin. Pleats in crystals on curved surfaces. *Nature*, 468(7326):947–951, dec 2010.

[18] Isaac R Bruss and Gregory M Grason. Non-euclidean geometry of twisted filament bundle packing. *Proceedings of the National Academy of Sciences of the United States of America*, 109(27):10781–10786, jul 2012.

[19] Christopher Joseph Burke, Badel Landry Mbanga, Zengyi Wei, Patrick T. Spicer, and Timothy J. Atherton. The role of curvature anisotropy in the ordering of spheres on an ellipsoid. *Soft Matter*, 11(29):5872–5882, 2015.

[20] Amar B. Pawar, Marco Caggioni, Roja Ergun, Richard W. Hartel, and Patrick T. Spicer. Arrested coalescence in Pickering emulsions. *Soft Matter*, 7(17):7710–7716, 2011.

[21] Henry Cohn, Yang Jiao, Abhinav Kumar, and Salvatore Torquato. Rigidity of spherical codes. *Geometry & Topology*, 15(4):2235–2273, 2011.

[22] S. Torquato and F. H. Stillinger. Jammed hard-particle packings: From Kepler to Bernal and beyond. *Reviews of Modern Physics*, 82(3):2633–2672, sep 2010.

[23] Aleksandar Donev, Salvatore Torquato, and Frank Stillinger. Pair correlation function characteristics of nearly jammed disordered and ordered hard-sphere packings. *Physical Review E*, 71(1):011105, jan 2005.

[24] Aleksandar Donev, Robert Connelly, Frank H. Stillinger, and Salvatore Torquato. Underconstrained jammed packings of nonspherical hard particles: Ellipses and ellipsoids. *Physical Review E - Statistical, Nonlinear, and Soft Matter Physics*, 75(5):1–32, 2007.

[25] Brian P. Flannery, Saul Teukolsky, William H. Press, and William T. Vetterling. *Numerical Recipes in C: The Art of Scientific Computing*. Cambridge University Press, 2007.

[26] T. S. Grigera, V. Martín-Mayor, G. Parisi, and P. Verrocchio. Phonon interpretation of the 'boson peak' in supercooled liquids. *Nature*, 422(6929):289–292, mar 2003.

[27] M. P. Allen and D. J. Tildesley. *Computer Simulations of Liquids*. Oxford University Press, New York, 1987.

[28] Peter Hilton and Jean Pedersen. The Euler Characteristic and Polya's Dream. *The American Mathematical Monthly*, 103(2):121–131, 1996.